Journal of Applied Physics

Fabrication and characterization of p^+-i-p^+ type organic thin film transistors with electrodes of highly doped polymer

Cite as: J. Appl. Phys. **119**, 154503 (2016); https://doi.org/10.1063/1.4946888
Submitted: 09 January 2016 . Accepted: 04 April 2016 . Published Online: 19 April 2016

Daisuke Tadaki, Teng Ma, Jinyu Zhang, Shohei Iino, Ayumi Hirano-Iwata, Yasuo Kimura, Richard A. Rosenberg, and Michio Niwano

ARTICLES YOU MAY BE INTERESTED IN

A simple method for controllable solution doping of complete polymer field-effect transistors
Applied Physics Letters **104**, 153304 (2014); https://doi.org/10.1063/1.4871096

High performance polythiophene thin-film transistors doped with very small amounts of an electron acceptor
Applied Physics Letters **92**, 063310 (2008); https://doi.org/10.1063/1.2883927

Organic electroluminescent diodes
Applied Physics Letters **51**, 913 (1987); https://doi.org/10.1063/1.98799

Lock-in Amplifiers
Find out more today

Zurich Instruments

© 2016 Author(s).

JOURNAL OF APPLIED PHYSICS 119, 154503 (2016)

Fabrication and characterization of p^+-i-p^+ type organic thin film transistors with electrodes of highly doped polymer

Daisuke Tadaki,[1,2,3] Teng Ma,[2,3] Jinyu Zhang,[2] Shohei Iino,[2] Ayumi Hirano-Iwata,[1,3] Yasuo Kimura,[3,4] Richard A. Rosenberg,[5] and Michio Niwano[2,3,a)]
[1]*Graduate School of Biomedical Engineering, Tohoku University, Sendai 980-8579, Japan*
[2]*Laboratory for Nanoelectronics and Spintronics, Research Institute of Electrical Communication, Tohoku University, Sendai 980-8577, Japan*
[3]*CREST, Japan Science and Technology Agency, Kawaguchi, Saitama 332-0012, Japan*
[4]*Tokyo University of Technology, Hachioji, Tokyo 192-0982, Japan*
[5]*Advanced Photon Source, Argonne National Laboratory, Lemont, Illinois 60439, USA*

(Received 9 January 2016; accepted 4 April 2016; published online 19 April 2016)

Organic thin film transistors (OTFTs) have been explored because of their advantageous features such as light-weight, flexible, and large-area. For more practical application of organic electronic devices, it is very important to realize OTFTs that are composed only of organic materials. In this paper, we have fabricated p^+-i-p^+ type of OTFTs in which an intrinsic (i) regioregular poly (3-hexylthiophene) (P3HT) layer is used as the active layer and highly doped p-type (p^+) P3HT is used as the source and drain electrodes. The 2,3,5,6-tetrafluoro-7,7,8,8-tetracyanoquinodimethane (F_4-TCNQ) was used as the p-type dopant. A fabricating method of p^+-i-p^+ OTFTs has been developed by using SiO_2 and aluminum films as capping layers for micro-scaled patterning of the p^+-P3HT electrodes. The characteristics of the OTFTs were examined using the photoelectron spectroscopy and electrical measurements. We demonstrated that the fabricated p^+-i-p^+ OTFTs work with carrier injection through a built-in potential at p^+/i interfaces. We found that the p^+-i-p^+ OTFTs exhibit better FET characteristics than the conventional P3HT-OTFT with metal (Au) electrodes, indicating that the influence of a carrier injection barrier at the interface between the electrode and the active layer was suppressed by replacing the metal electrodes with p^+-P3HT layers. *Published by AIP Publishing.*
[http://dx.doi.org/10.1063/1.4946888]

I. INTRODUCTION

Organic thin film transistors (OTFTs) have been explored because they have a potential to realize light-weight, flexible, and large-area electronic devices.[1–4] For practical application of OTFTs to electronic devices, it is very important to realize OTFTs that are composed only of organic materials. Since, for the conventional OTFTs, metallic materials such as gold (Au) and aluminum (Al) are generally utilized as the source and drain electrodes, which may increase the fabrication cost. Furthermore, the electrical performance of OTFTs depends on both the charge density at the channel region and the carrier injection barrier residing at the metal/organic layer interface. Especially, influence of the carrier injection barrier will be enhanced as the channel length is reduced. This may lead to a decrease in the apparent carrier mobility of OTFTs.[5–10] Therefore, in order to reduce the fabrication cost and to improve the performance of OTFTs, we need to develop new types of all-organic OTFTs that are less affected by carrier injection barriers at the interface between the metal electrode and the active layer.

Molecular doping is a technique which is well known as a charge-transfer process intended to improve the performance of organic electronic devices. Previously, it has been reported that when a doped organic layer is inserted between the electrode and the emission layer in OLEDs, carrier injection from the electrode is improved, leading to a notable increase in the carrier conductivity of the transport layer.[11–16] Furthermore, it has been revealed that the electrical performance of OTFTs with metal electrodes is improved when a p-type dopant material, such as 2,3,5,6-tetrafluoro-7,7,8,8-tetracyanoquinodimethane (F_4-TCNQ), $FeCl_3$, or NPD-9 is used at the metal/organic layer interface (the so-called contact doping), where the carrier density is modified to improve the carrier injection characteristics at the metal/organic layer interface, reducing the contact resistance.[17–21] For these cases, however, the carrier injection barrier at metal/organic layer interfaces, which strongly depends on the chemical state of the metal electrode surface, remains intact.

In this study, we apply the molecular doping technique to fabricate a p^+-i-p^+ type of OTFT in which highly doped p-type organic layers are used as the source and drain electrodes, instead of the conventional metal electrodes such as Au and Al. Previously, OTFTs with organic (modified PEDOT-PSS) electrodes have been proposed which work on the almost same level with the OTFT with Au electrodes.[22] The difference between our proposed transistor and the conventional one is that we use the same organic polymer, regioregular poly (3-hexylthiophene) (P3HT, band gap = 2.3 eV (Ref. 23)), for both the electrode and the active layer, as depicted in Fig. 1(a). The Fermi level of the doped polymer electrodes differs from that of the active layer, depending on the dopant concentration (Fig. 1(b)). As shown in Fig. 1(c), a built-in

a)Author to whom correspondence should be addressed. Electronic mail: niwano@riec.tohoku.ac.jp

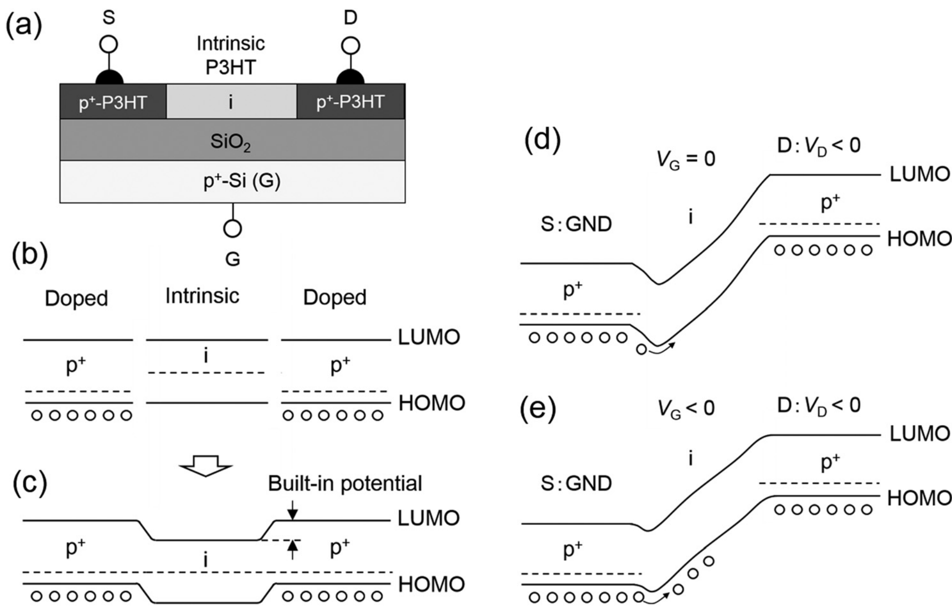

FIG. 1. (a) Cross sectional view of a p^+-i-p^+ OTFT. Energy diagrams of (b) isolated p^+ and intrinsic (i) layers, and (c) the p^+-i-p^+ OTFT in the thermal equilibrium. Energy diagrams of the OTFT under active modes of operation; (d) $V_{GS} = 0$, $V_{DS} < 0$ and (e) $V_{GS} < 0$, $V_{DS} < 0$.

potential is formed between the highly doped layer and the intrinsic layer. The drain current (I_D) of this OTFT can be tuned by changing the gate voltage (V_{GS}), as shown in Figs. 1(d) and 1(e). We use F_4-TCNQ as the p-type dopant in the P3HT layer, because it has an extremely high electron-accepting nature.[24–29] We examined the electrical characteristics of the interface of the intrinsic P3HT layer and the F_4-TCNQ-doped P3HT layers using synchrotron-radiation photoemission spectroscopy (SR-PES). In order to fabricate a prototype of p^+-i-p^+ OTFT in which a highly doped (p^+) P3HT layer is used as source and drain electrodes, we have developed a pattering method for organic layers using SiO_2 and aluminum capping layers. We demonstrated that the fabricated OTFTs work and showed better characteristics than the conventional bottom-contact P3HT-OTFT with Au electrodes. This suggests that the influence of carrier injection through the so-called Schottky barrier at the interface between the metal electrode and the active layer can be suppressed by replacing the metal electrode with p^+-P3HT layer. However, the fabricated OTFTs exhibited undesired deterioration in FET characteristics after post-annealing or long-term operation. We will discuss the cause of the deterioration and the ways to suppress the deterioration.

II. FABRICATION OF p^+-i-p^+ OTFT

A. Structure of p^+-i-p^+ OTFT

We fabricated a p^+-i-p^+ type of OTFT in which highly doped (p^+) P3HT layers were used as source and drain electrodes, as illustrated in Fig. 2(a). A 250-nm thick SiO_2 layer was formed by RF-sputtering on a SiN-covered p-Si substrate. The surface of the oxide was treated with hexamethyldisilane (HMDS). A 5 wt. %-doped P3HT layer was then formed by spin-coating a F_4-TCNQ-containing P3HT solution (in chloroform with 5 mg/ml), and subsequently annealing at 100 °C for 5 min under dry N_2 ambient. In order to form the source and drain electrodes, the doped P3HT layer was patterned by the photolithographic method that will be described in Subsection II B. Next, the patterned p^+-P3HT electrode was etched by photolithographic methods as described in Subsection II C, to form the channel region and the source/drain electrodes. Finally, a non-doped P3HT layer that functioned as the active layer was formed by drop-casting an intrinsic 3 μl P3HT solution (in chloroform with 5 mg/ml) on the middle portion between the source and drain electrodes. In Fig. 2(b), we depict the cross sectional view of the channel region. The doped layer was completely covered with SiO_2, and the area where the p^+ and i-P3HT layers contacted with each other was minimized. This structure is beneficial to suppress an undesired leakage path. The channel length was varied from 30 μm to 550 μm, and the channel width was set at approximately 1 mm. Figure 2(c) shows a top view of the fabricated p^+-i-p^+ OTFTs.

B. Patterning of p^+-P3HT layers

Here, we propose a method of pattering organic thin layers by the photolithographic method. The highly doped P3HT (p^+-P3HT) layer was patterned by the procedure as depicted in Fig. 3. We utilized SiO_2 and aluminum films as the mask layers for photolithographic patterning. Previously, some researchers have investigated a photolithographic method for patterning P3HT layers.[30,31] Jia and coworkers[31] have proposed a patterning process which is compatible with plastic substrates and P3HT layers. Since the organic semiconductor is sensitive to water, oxygen, and solvents, photoresist cannot be applied in direct contact with the organic layer. Therefore, a protective capping layer must be deposited on top of the organic layer before photoresist processing. In their process, parylene and Al_2O_3 by atomic layer deposition (ALD) were used as capping layers. In our method, we utilized SiO_2 layers as the capping and protective layer. We firstly deposited a thin SiO_2 layer with a thickness of approximately 5 nm on the p^+-P3HT layer by a vacuum evaporation method. The SiO_2 layer functioned as the protective capping layer to prevent the surface of the p^+-P3HT layer from being damaged in subsequent processing. In order to suppress

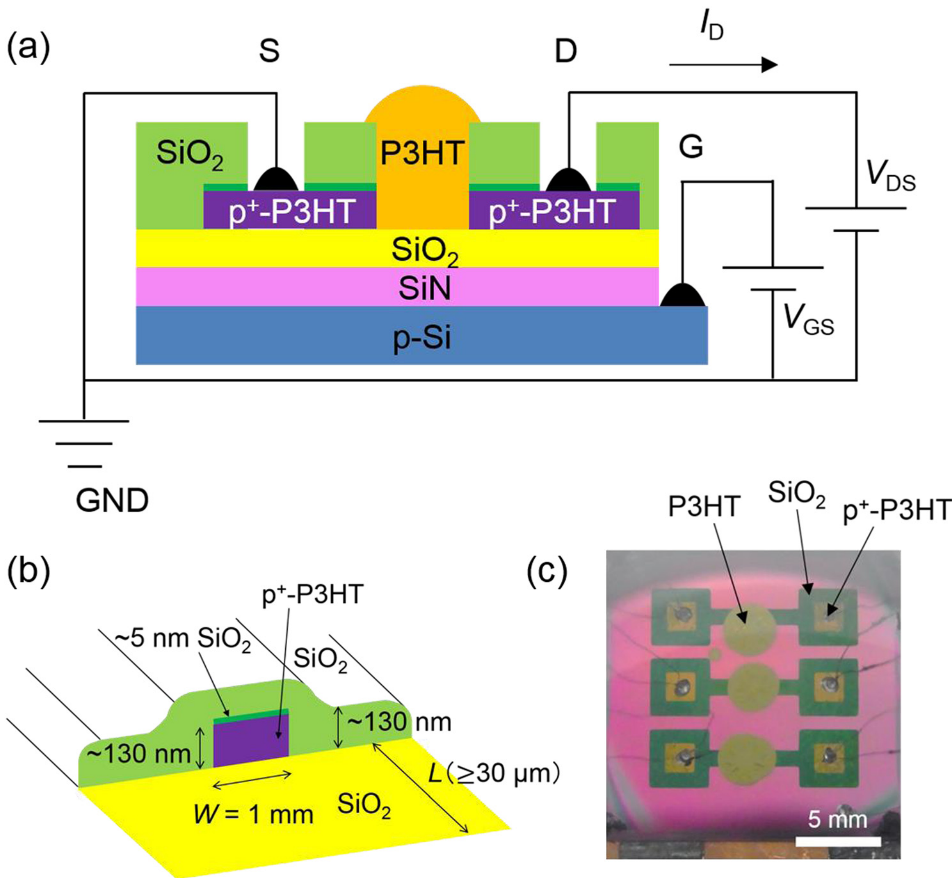

FIG. 2. (a) Structure of the fabricated OTFT in which highly doped (p^+) P3HT layers are used as source/drain electrodes. (b) Cross sectional view of the channel region and (c) top view of the fabricated p^+-i-p^+ OTFTs.

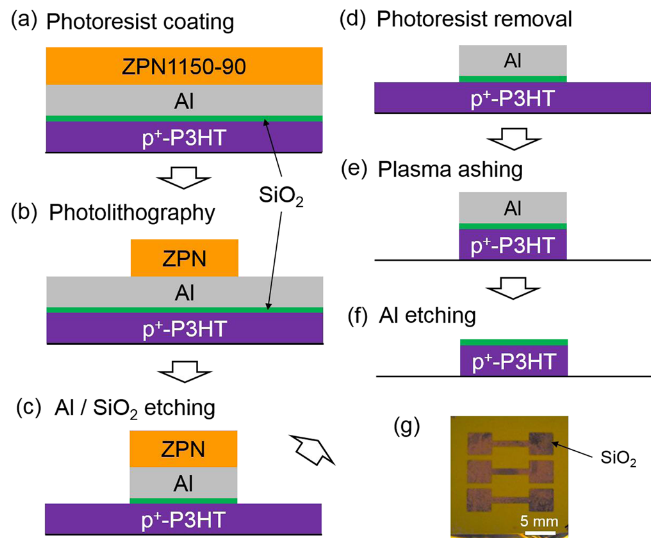

FIG. 3. (a)–(f) Procedure for patterning of the p^+-P3HT layer. (g) Top view of the patterned p^+-P3HT layers that are covered with a thin layer of SiO_2.

undesired reactions of the SiO_2 capping layer with the underlying p^+-P3HT organic layer, the p^+-P3HT layer was positioned more than 40 cm apart from the source during the SiO_2 evaporation, keeping the surface temperature as low as possible, that is, below about 200 °C. After that, we formed a thin aluminum layer, approximately 80 nm thick, by a vacuum evaporation method. Next, photoresist (ZPN1150-90, Zeon Corporation) was spin-coated on the Al capping layer, as shown in Fig. 3(a), and then was patterned by the photolithographic method, as shown in Fig. 3(b). The uncovered portion of the Al and SiO_2 capping layers was etched away by a phosphoric acid solution and a buffered HF solution that contains ammonium fluoride, respectively, as shown in Fig. 3(c). Subsequently, the photoresist overlayer was removed by a commercial remover (ZS-50, Zeon Corporation) to form patterned Al mask layers, as shown in Fig. 3(d). The portions of the p^+-P3HT layer that were not covered by the Al mask were removed by the O_2 plasma ashing (Fig. 3(e)). Finally, the Al mask layers were removed by a phosphoric acid solution to form the patterned p^+-P3HT layer covered with the thin layer of SiO_2, as shown in Figs. 3(f) and 3(g).

C. Formation of the channel of p^+-i-p^+ OTFT

The channel region of a p^+-i-p^+ type of OTFT was formed according to the procedure shown in Fig. 4. First, we covered the p^+-P3HT layer with a spin-on-glass (SOG)-SiO_2 layer and a photoresist (OFPR-800LB 20 cP, TOKYO OHKA KOGYO Co., Ltd.) layer, as shown in Fig. 4(a). The thickness of the SOG layer was approximately 130 nm that is formed by spin-coating of organic solvent-based solution (SSN-SD2000, Exousia Inc.) and subsequently annealing at 100 °C for 5 min. Next, we utilized the photolithographic method to form the open window in the SOG-SiO_2 film on the p^+-P3HT layer, where the channel was to be formed, as shown in Figs. 4(b) and 4(c). Then, the p^+-P3HT layer in the open window region was removed by O_2 plasma ashing

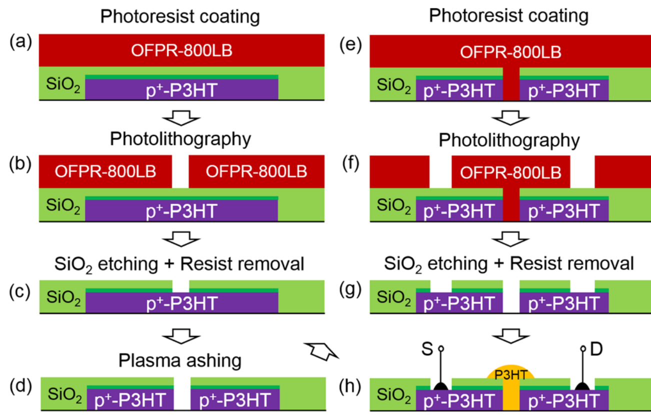

FIG. 4. Procedure for the formation of the channel region of the p^+-i-p^+ OTFT.

to separate the p^+-P3HT layer into two parts, as shown in Fig. 4(d): one is the source electrode and the other is the drain electrode. In order to attach the leading wires to the two electrodes, a window was opened on each electrode by the photolithographic method, as shown in Figs. 4(e) through 4(g). After removing the photoresist, the bottom SiO_2 substrate was treated with HMDS again to form a hydrophobic surface, and the patterned p^+-P3HT layers were annealed at 125 °C for 15 min to evaporate the residual solvent. Finally, a 3 μl P3HT solution was drop-casted on the channel region to form the active layer, and the leading wires were attached to the source/drain electrodes (Fig. 4(h)).

The key point in the channel formation process was the structure of the channel region after the removal of the p^+-P3HT layer by O_2 plasma ashing; that is, the structural profile as depicted in Figs. 2(b) and 4(d). We therefore examined in detail the structural profile of the channel region by a confocal laser scanning microscope with a laser wavelength of 405 nm. Figure 5 shows the typical optical images of the channel region. Figures 5(a), 5(b), and 5(c) show a top view of the channel region, a cross sectional depth profile along the dashed line in Fig. 5(a), and a three-dimensional image of the channel region, respectively. Note that the images and profile are by about 50 times magnified in the vertical direction. The depth profile of Fig. 5(b) indicates that the p^+-P3HT layer was approximately 130 nm thick, which is almost the same as the thickness of the as-deposited film. We notice that the SOG-SiO_2 capping layer on the p^+-P3HT layer was about 30 nm in thickness, which should be compared to the initial thickness of the as-formed SOG layer, about 130 nm. It seems that the SOG-SiO_2 layer was partially etched by O_2-plasma. However, we determined that the 30 nm thick SOG-SiO_2 layer functions as an interlayer insulation film. Close inspection of Fig. 5 indicates that the p^+-P3HT layers without an SiO_2 capping layer appeared at the edge of the channel regions. Indeed, energy-dispersive x-ray analysis (EDX) measurements demonstrated that at those uncovered regions, emission of the C kα characteristic x-ray which is originated from P3HT was identified. We suspect that during O_2-plasma ashing, the SOG-SiO_2 capping layer partially peeled from the p^+-P3HT layer and shrank at edge regions.

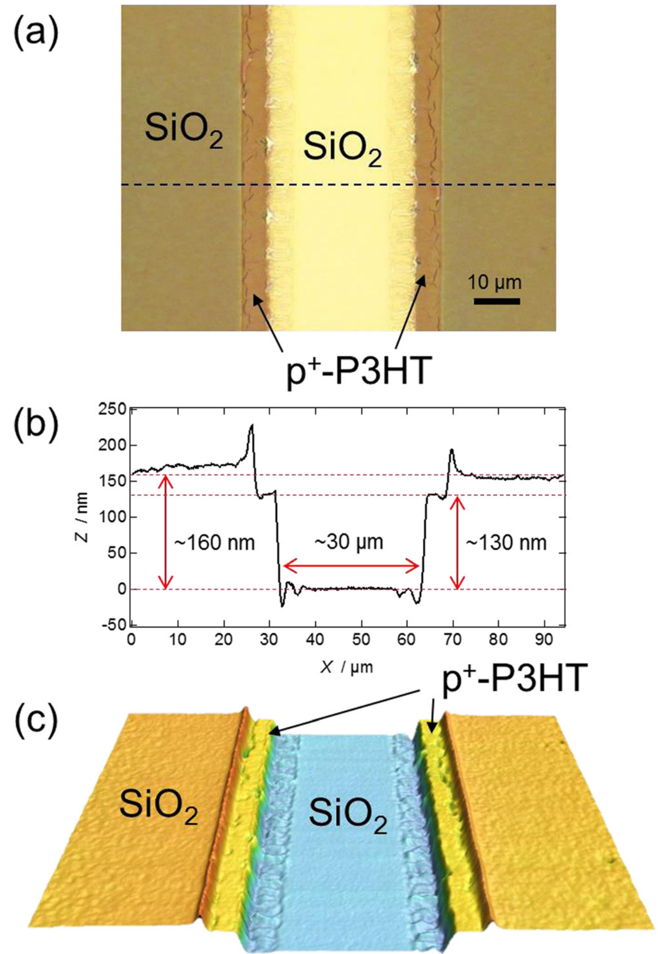

FIG. 5. (a) Top view of the channel region, (b) cross sectional depth profile along the dashed line in Fig. 5(a), and (c) three-dimensional image of the channel region. Note that the images and profile are by about 50 times magnified in the vertical direction.

III. RESULTS AND DISCUSSION

A. Built-in potential at the p^+/i interface

In order to estimate the height of the built-in potential at the p^+/i interface, as shown in Fig. 1(c), we have measured C 1s and S 2p photoemission spectra for F_4-TCNQ-doped P3HT samples with different doping concentrations. Synchrotron-radiation photoemission measurements were performed at beamline 4-ID-C at the Advanced Photon Source (APS) using 650 eV x-rays, and a Scienta Omicron Argus electron energy analyzer. The angle of incidence between the x-rays and the sample normal was 60°. Samples were mounted using double sided carbon tape, and silver paint was used to ground the surface of the samples to the holder. All binding energies are referenced to the Ag $3d_{5/2}$ peak at 368.3 eV. In order to determine the dependence of the Fermi level of F_4-TCNQ-doped P3HT layers on the doping concentration of F_4-TCNQ, we prepared F_4-TCNQ-doped P3HT layers with different dopant concentrations. We spin-coated the F_4-TCNQ-containing P3HT solution on the Si substrate, followed by annealing under the same conditions as mentioned above. Figure 6(a) shows typical C 1s and S 2p core-level photoemission spectra for different

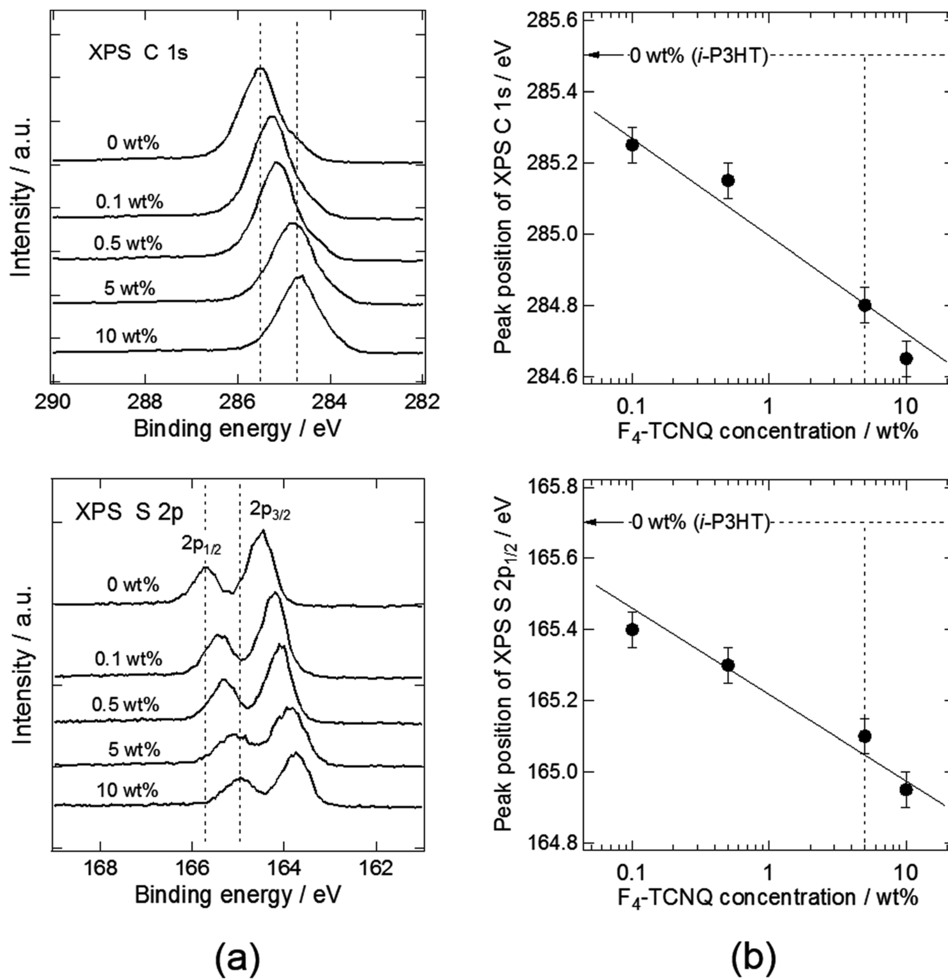

FIG. 6. (a) C 1s and S 2p photoemission spectra of P3HT layers with different concentrations of F_4-TCNQ dopant. (b) Binding energy of the C 1s and S $2p_{1/2}$ core-level as a function of F_4-TCNQ concentration.

dopant concentrations. We can clearly see that the binding energy of both the C 1s and S 2p core-level decreases with increase in dopant concentration, indicating that the ionization potential, which corresponds to the HOMO level of the doped P3HT layer, decreases as the dopant concentration increases. This is in agreement with the previous results.[32,33] Therefore, we can expect that a potential barrier forms when the intrinsic and doped layers of P3HT contact with each other. This potential barrier can be regarded as the hole-injection barrier at the p^+/i interface, as shown in Fig. 1(c). In Fig. 6(b), we plot the binding energy of the C 1s and S $2p_{1/2}$ core-level as a function of dopant concentration. It is evident that the shift of the binding energy, i.e., the Fermi level shift, is proportional to a logarithm of the dopant concentration, as we expected. This suggests that the electrons effectively moved from P3HT to F_4-TCNQ; that is, the charge-transfer process almost completely occurred in the complex of P3HT and F_4-TCNQ. Furthermore, the result of Fig. 6(b) shows that the potential barrier at the p^+/i interface should be approximately 0.7 eV for a dopant concentration of 5 wt. %. Considering that the gap energy between the HOMO and LUMO level of P3HT is about 2 eV,[23] we can expect that this potential barrier functions as the hole-injection barrier at the p^+/i interface. Conductivity of p^+-layers is another important factor in fabricating p^+-i-p^+ type of OTFTs. Previously, we have measured the conductivity of p^+-P3HT layers doped with F_4-TCNQ by using the four-probe method.[34] We found that the conductivity was proportional to the square of the dopant concentration at high dopant levels.[34] Unfortunately, even at high dopant concentrations around 10 wt. %, the conductivity of p^+-P3HT layers was approximately 10^{-2} S/cm, which is much less than that of PEDOT-PSS, typically 1–10 S/cm. However, the main purpose of this study is to form the p^+-i-p^+ structures that are made from the same organic material. In addition, at high dopant concentrations around 10 wt. %, aggregation of F_4-TCNQ molecules readily occurred. We therefore used a p^+-P3HT layer with 5 wt. % concentration, which has a conductivity of around 3×10^{-3} S/cm, as the source and drain electrodes in our p^+-i-p^+ type of OTFTs.

B. Characteristics of the p^+-i-p^+ OTFTs

In Figs. 7(a) through 7(c), we show the electrical characteristics of p^+-i-p^+ OTFTs with three different channel lengths. A gate voltage was applied to the p^+-Si substrate as shown in Fig. 2(a). As mentioned above, we used highly doped P3HT as source/drain electrodes in our OTFTs. We can see that the OTFT exhibits typical p-type FET operation as expected. At a gate voltage (V_{GS}) of -20 V and a source-drain voltage (V_{DS}) of -20 V, the drain current (I_D) was almost in the same order as that observed for the conventional bottom-contact P3HT-OTFT that we fabricated by using metal (Au) as the electrodes shown in Fig. 7(d).

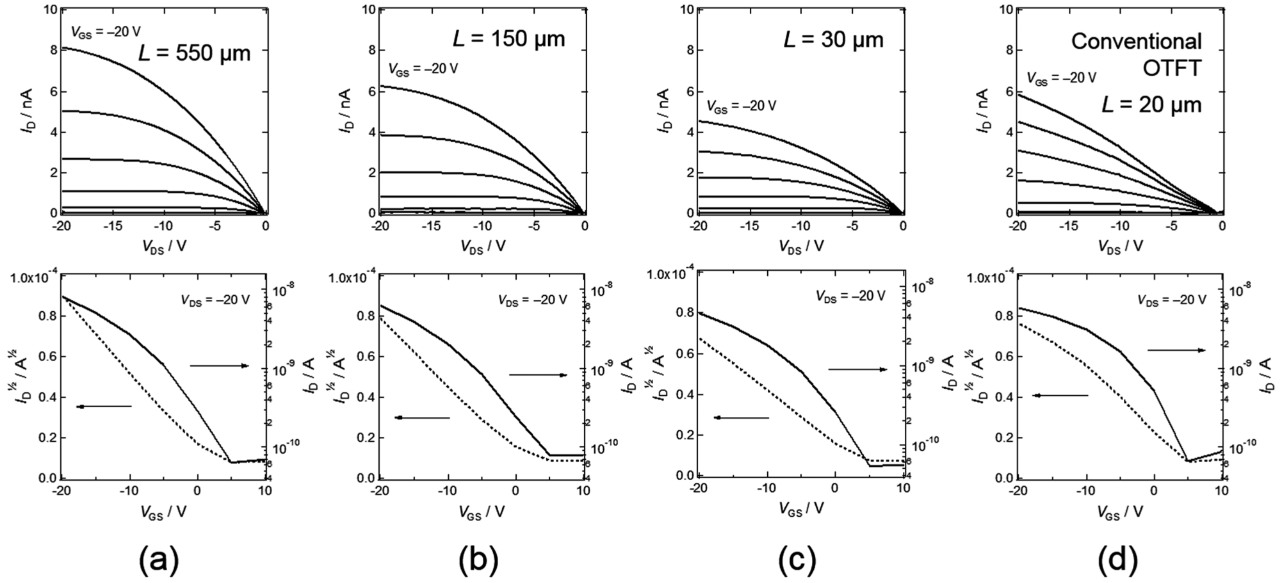

FIG. 7. Output and transfer characteristics of the p^+-i-p^+ type of OTFTs for three different channel lengths: (a) 550, (b) 150, and (c) 30 μm and (d) those of the conventional bottom-contact P3HT-OTFT with metal (Au) electrodes ($L = 20\ \mu$m).

In Fig. 8, we plot the apparent mobility evaluated from the transfer characteristic of the OTFTs with different channel lengths as the closed circle. We can see in Fig. 8 that the carrier (hole) mobility decreased with the decrease of the channel length, which is the similar trend as that observed for conventional OTFTs with metal electrodes.[5–10] We suspect that the observed decrease in the carrier mobility is more or less due to the influence of a carrier injection barrier at the p^+/i interfaces. At a channel length of 20–30 μm, however, the apparent mobility for the p^+-i-p^+ OTFTs is an order of magnitude higher than that for the conventional bottom-contact P3HT-OTFT with Au electrodes as indicated by an open circle in Fig. 8. From this result, we interpret that the influence of a potential barrier at the p^+/i interfaces is significantly suppressed as compared to the conventional metal/organic interfaces. In order to give support to our interpretation, we estimated the contact resistance (R_c) at the p^+/i interfaces by using the transfer line method (TLM). In Fig. 9, we plot the total resistance (R) as a function of channel length. The total resistances have been derived from the output characteristics of the OTFTs as shown in Fig. 7. In the inset of Fig. 9, we plot the contact resistance that is the y-intercept value obtained by extrapolating the straight lines (dotted lines) to $L = 0$. We confirmed that the resistance of the p^+ bulk layer and the contact wire/p^+ interface is less than 0.1 GΩcm. This implies that the attachment of contact wires to the p^+-layers does not significantly affect the electrical performance of the OTFTs. Thus, we can determine from the result of Fig. 9 that the contact resistance of the p^+-i-p^+ OTFTs is almost half of

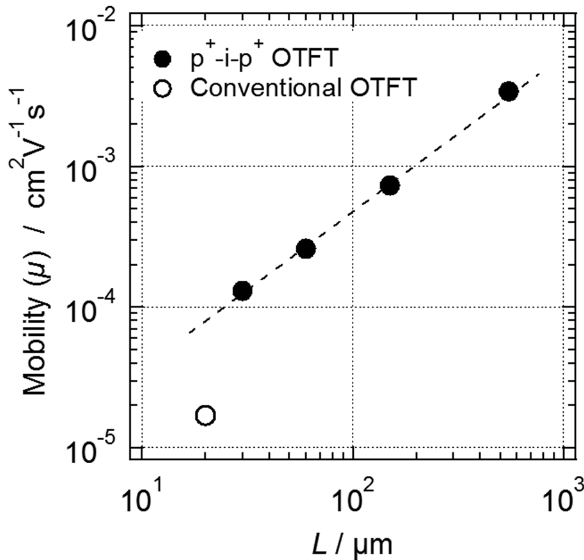

FIG. 8. Carrier mobility as a function of channel length of the p^+-i-p^+ OTFT as the closed circle of the conventional bottom-contact P3HT-OTFT with metal (Au) electrodes as the open circle, respectively.

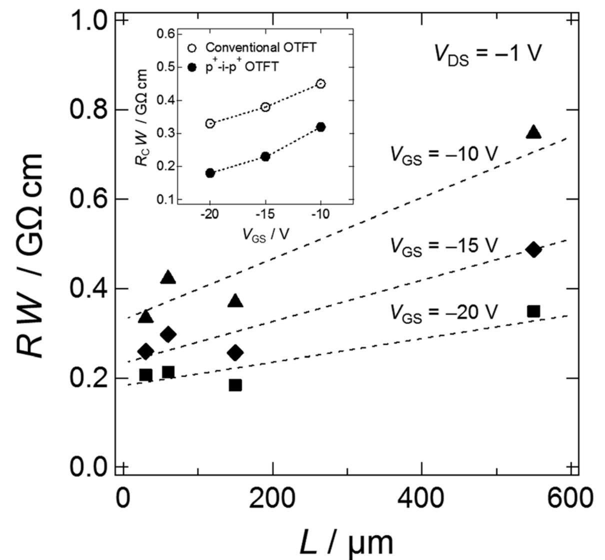

FIG. 9. Total resistance of the p^+-i-p^+ OTFT for different channel lengths ($V_{GS} = -1$ V, and each channel width (W) is set as 1 mm) and contact resistance (inset) estimated from the transfer line method (TLM).

that of the conventional bottom-contact P3HT-OTFT with Au electrodes.

As mentioned above, the active layer of P3HT was formed by drop-casting a chloroform solution of P3HT on the channel region and subsequently drying it at room temperature under dry N_2 environment. The FET characteristics of the OTFTs fabricated with channel lengths $L = 550\,\mu m$ and $30\,\mu m$ are shown in Fig. 10(a), which are the same as those shown in Figs. 7(a) and 7(c), though the scales of the vertical axes are partly different. In the formation process of the active layer, we once annealed the drop-casted P3HT layer at 125 °C for 15 min after drying the layer. Figure 10(b) shows the FET characteristics of the annealed OTFTs. For a channel length of $30\,\mu m$, it is evident that the post-annealed OTFT did not work, exhibiting an ohmic behavior. It was suspected that during post-annealing, F_4-TCNQ dopants migrated from the highly doped P3HT electrode into the P3HT active layer, resulting in the formation of a lightly doped P3HT layer between the source and drain electrodes. In order to give the evidence to the dopant migration at p^+/i interfacial regions at elevated temperatures, we have performed EDX on the post-annealed interface. We measured the lateral distribution in the p^+/i interfacial regions of the intensity of the F kα characteristic x-ray that comes only from F_4-TCNQ molecules. As a result, we found that the F_4-TCNQ dopants diffuse to at least $20\,\mu m$ away from each side of the interfaces after post-annealing at 125 °C for 15 min. This observation suggests that for OTFTs having a channel length of $30\,\mu m$, the whole part of the active layer will be doped with F_4-TCNQ. OTFTs with channel lengths of $550\,\mu m$, on the other hand, exhibited slight changes in the FET characteristics by post-annealing. This implies that the dominant part of the intrinsic layer in the channel region remained undoped, though slightly doped layers were formed at interfacial regions. Accordingly, we determine that F_4-TCNQ is mobile in P3HT layers at elevated temperatures. We interpret that even when the active layer was formed by drying the drop-casted P3HT at room temperature, F_4-TCNQ slightly migrated from the p^+-P3HT electrodes to the intrinsic layer.

In order to examine the stability of the characteristics of the p^+-i-p^+ OTFTs, we have carried out a series of measurements of FET characteristics several times for the OTFTs as shown in Fig. 10(a). We observed that whenever we repeated a series of measurements, the characteristic of the OTFT gradually deteriorated. In Fig. 10(c), we show the FET characteristics of the OTFT collected after performing a series of measurements four times for the OTFTs in Fig. 10(a). The change was occurred in a channel length of $30\,\mu m$, while it was slightly occurred in that of $550\,\mu m$. For the channel length of $30\,\mu m$, it is obvious from a comparison of Figs. 10(b) and 10(c) that the characteristic of being measured four times is quite similar to that observed for the annealed OTFT. This suggests that the dopant migration occurred during the operation of OTFTs. We suspect that during the course of OTFT operation, negatively charged F_4-TCNQ dopants migrated from the negatively biased drain electrode to the active layer. On the other hand, for the OTFTs with channel length of $550\,\mu m$, slight changes in the characteristics were observed during the FET operation. This indicates

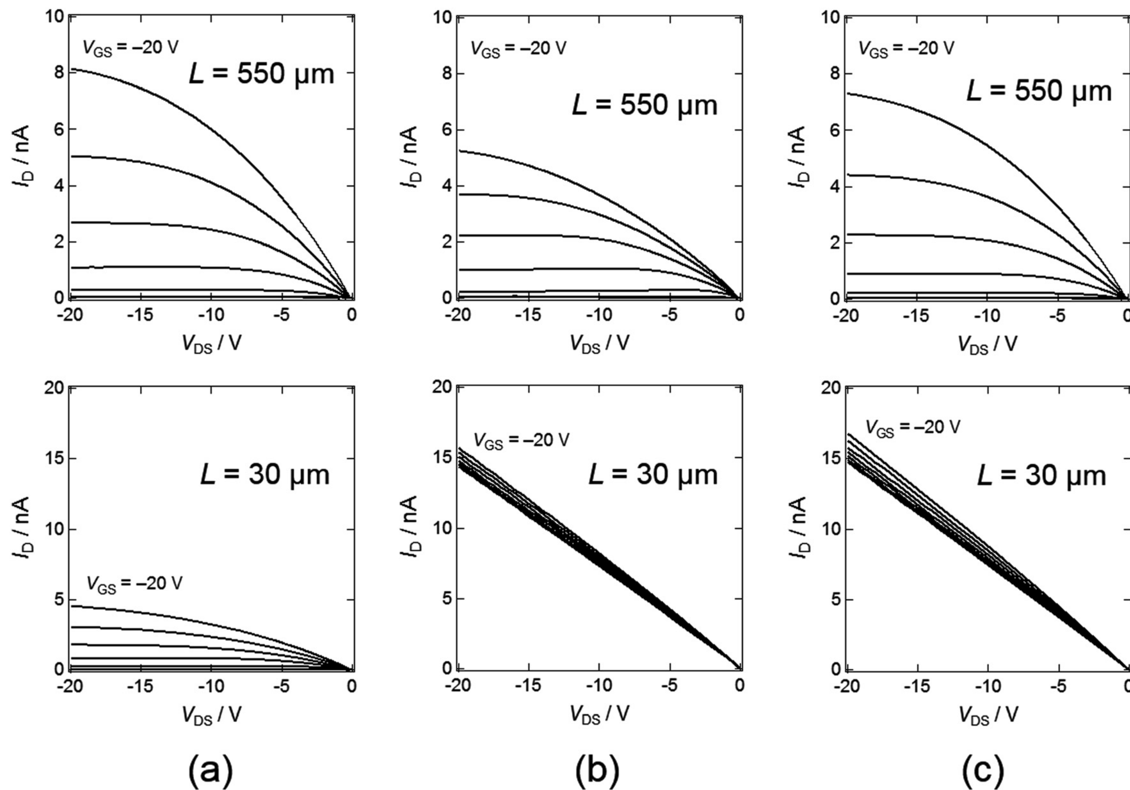

FIG. 10. Output characteristics of the p^+-i-p^+ OTFT with channel lengths of $550\,\mu m$ and $30\,\mu m$ with (a) as-deposited and (b) post-annealed P3HT active layers. (c) Output characteristic of the p^+-i-p^+ OTFT after fourth run of a series of FET measurements.

that the intrinsic, undoped layer remained intact in the dominant part of the channel region, though slightly doped layers would be formed at the interfacial regions.

As described above, we found that the F_4-TCNQ dopant molecule is easy to migrate in the P3HT layer, leading to the deterioration in the performance of p^+-i-p^+ OTFTs such as the temporal change in the characteristics of the OTFTs. This deterioration was remarkably observed especially for OTFTs with short channel lengths. In order to improve the performance of p^+-i-p^+ type of OTFTs, therefore, we need to suppress the migration of dopants. One possible way to suppress the dopant migration would be to develop the immobile dopants, for example, a dopant molecule with larger molecular weight. Another way would be to use an effective barrier layer to prevent the dopant migration at p^+/i interfaces. Typical inorganic barrier layers would be SiO_2, SiN_x, Al_2O_3, or Al.[35] We have tried to suppress the dopant migration by using a thin SiO_2 layer as the blocking layer. However, the preliminary results showed that the SiO_2 layer was not effective for blocking the dopant migration. Further studies are needed to develop an effective method for suppressing the dopant migration.

IV. CONCLUSION

We have fabricated a p^+-i-p^+ type of OTFT in which an intrinsic (i) regioregular P3HT layer is used as the active layer and a highly doped p-type (p^+) layer of P3HT is used as the source and drain electrodes. F_4-TCNQ was used as the p-type dopant. A new method of micro-scaled patterning of the p^+-organic electrodes has been developed by using thin SiO_2 and aluminum films as capping or mask layers. We demonstrated that the fabricated p^+-i-p^+ OTFTs work with the carrier injection through a built-in potential at p^+/i interfaces. We found that the p^+-i-p^+ OTFTs exhibit better FET characteristics than the conventional P3HT-OTFT with metal (Au) electrodes, indicating that the influence of a carrier injection barrier at the interface between the electrode and the active layer was suppressed by replacing the metal electrodes with p^+-P3HT layers.

The present results demonstrated that the p^+-i-p^+ OTFT we proposed here is feasible and will enable the realization of a new type of organic transistor; for example, all-organic flexible transistors that can be fabricated by printing processes. However, it should be noted that the dopant migration or interdiffusion of organic materials at interfaces of OTFTs will be the problem we have to address in fabricating such all-organic TFTs by printing processes such as an inkjet printing method.

ACKNOWLEDGMENTS

We would like to thank Scienta Omicron for the loan of the Argus electron energy analyzer. This work has been performed at the Laboratory for Nanoelectronics and Spintronics, Research Institute of Electrical Communication, Tohoku University, and partly at Advanced Photon Source, Argonne National Laboratory. The work performed at the Advanced Photon Source was supported by the U.S. Department of Energy, Office of Science, Office of Basic Energy Sciences under Contract No. DE-AC02-06CH11357. This work was supported in part by CREST program (Development of Atomic or Molecular Two-Dimensional Functional Films and Creation of Fundamental Technologies for Their Applications) of Japan Science and Technology Agency (JST).

[1] T. Sekitani, U. Zschieschang, H. Klauk, and T. Someya, Nat. Mater. **9**, 1015 (2010).
[2] H. U. Khan, M. E. Roberts, W. Knoll, and Z. Bao, Chem. Mater. **23**, 1946 (2011).
[3] D. K. Hwang, C. Fuentes-Hernandez, J. B. Kim, W. J. Potscavage, Jr., and B. Kippelen, Org. Electron. **12**, 1108 (2011).
[4] S. Steudel, K. Myny, S. Schols, P. Vicca, S. Smout, A. Tripathi, B. van der Putten, J. van der Steen, M. van Neer, F. Schütze, O. R. Hild, E. van Veenendaal, P. van Lieshout, M. van Mil, J. Genoe, G. Gelinck, and P. Heremans, Org. Electron. **13**, 1729 (2012).
[5] J. Zaumseil, K. W. Baldwin, and J. A. Rogers, J. Appl. Phys. **93**, 6117 (2003).
[6] D. J. Gundlach, L. Zhou, J. A. Nichols, T. N. Jackson, P. V. Necliudov, and M. S. Shur, J. Appl. Phys. **100**, 024509 (2006).
[7] Y. Kimura, T. Oba, N. Shimakura, and M. Niwano, Appl. Phys. Lett. **94**, 073303 (2009).
[8] Y. Chen and I. Shih, J. Mater. Sci. **44**, 280 (2009).
[9] Y. Xu, R. Gwoziecki, I. Chartier, R. Coppard, F. Balestra, and G. Ghibaudo, Appl. Phys. Lett. **97**, 063302 (2010).
[10] H. Kleemann, A. A. Zakhidov, M. Anderson, T. Menke, K. Leo, and B. Lüssem, Org. Electron. **13**, 506 (2012).
[11] X. Zhou, M. Pfeiffer, J. Blochwitz, A. Werner, A. Nollau, T. Fritz, and K. Leo, Appl. Phys. Lett. **78**, 410 (2001).
[12] J. Huang, M. Pfeiffer, A. Werner, J. Blochwitz, K. Leo, and S. Liu, Appl. Phys. Lett. **80**, 139 (2002).
[13] M. Pfeiffer, K. Leo, X. Zhou, J. S. Huang, M. Hofmann, A. Werner, and J. Blochwitz-Nimoth, Org. Electron. **4**, 89 (2003).
[14] C. C. Chang, M. Hsieh, and J. Chen, Appl. Phys. Lett. **89**, 253504 (2006).
[15] F. Wang, X. Qiao, T. Xiong, and D. Ma, Org. Electron. **9**, 985 (2008).
[16] H. Z. Siboni and H. Aziz, Org. Electron. **14**, 2510 (2013).
[17] Y. Abe, T. Hasegawa, Y. Takahashi, T. Yamada, and Y. Tokura, Appl. Phys. Lett. **87**, 153506 (2005).
[18] F. Fujimori, K. Shigeto, T. Hamano, T. Minari, T. Miyadera, K. Tsukagoshi, and Y. Aoyagi, Appl. Phys. Lett. **90**, 193507 (2007).
[19] J. Frisch, H. Glowatzki, S. Janietz, and N. Koch, Org. Electron. **10**, 1459 (2009).
[20] Y. Wakatsuki, K. Noda, Y. Wada, T. Toyabe, and K. Matsushige, J. Appl. Phys. **110**, 054505 (2011).
[21] F. Ante, D. Kälblein, U. Zschieschang, T. W. Canzler, A. Werner, K. Takimiya, M. Ikeda, T. Sekitani, T. Someya, and H. Klauk, Small **7**, 1186 (2011).
[22] F. Xue, Y. Su, and K. Varahramyan, IEEE Trans. Electron Devices **52**, 1982 (2005).
[23] A. Assadi, C. Svensson, M. Willander, and O. Inganäs, Appl. Phys. Lett. **53**, 195 (1988).
[24] K. H. Yim, G. L. Whiting, C. E. Murphy, J. J. M. Halls, J. H. Burroughes, R. H. Friend, and J. Kim, Adv. Mater. **20**, 3319 (2008).
[25] L. Ma, W. H. Lee, Y. D. Park, J. S. Kim, H. S. Lee, and K. Cho, Appl. Phys. Lett. **92**, 063310 (2008).
[26] P. Pingel, L. Zhu, K. S. Park, J. Vogel, S. Janietz, E. Kim, J. P. Rabe, J. Brédas, and N. Koch, J. Phys. Chem. Lett. **1**, 2037 (2010).
[27] P. Pingel, R. Schwarzl, and D. Neher, Appl. Phys. Lett. **100**, 143303 (2012).
[28] P. Pingel and D. Neher, Phys. Rev. B **87**, 115209 (2013).
[29] D. T. Duong, C. Wang, E. Antono, M. F. Toney, and A. Salleo, Org. Electron. **14**, 1330 (2013).
[30] C. Balocco, L. A. Majewski, and A. M. Song, Org. Electron. **7**, 500 (2006).
[31] H. Jia, E. K. Gross, R. M. Wallace, and B. E. Gnade, Org. Electron. **8**, 44 (2007).
[32] S. Olthof, W. Tress, R. Meerheim, B. Lüssem, and K. Leo, J. Appl. Phys. **106**, 103711 (2009).
[33] H. Hintz, H. Peisert, H.-J. Egelhaaf, and T. Chassé, J. Phys. Chem. C **115**, 13373 (2011).
[34] D. Tadaki, T. Ma, J. Zhang, S. Iino, A. Hirano-Iwata, Y. Kimura, and M. Niwano, Jpn. J. Appl. Phys., Part 1 **54**, 091602 (2015).
[35] J. S. Lewis and M. S. Weaver, IEEE J. Sel. Top. Quantum Electron. **10**, 45 (2004).